Effects of Ignition Location on Soot and Species Formation through Tracking Flame Light Emission and Temperature

Yiran Wang [a], Zhen Ma [a], Yang Zhang [a] (✉)
[a] Department of Mechanical Engineering, the University of Sheffield
Sheffield, UK

1 Introduction

The ignition process of a flammable gas mixture is a complicated chemical reaction depending on many parameters such as temperature, pressure and flame propagation velocity. Further investigation of the ignition process with respect to ignition timing and location is highly desirable for many combustion devices, particularly in spark-ignition (SI) engines. It has been demonstrated that ignition location strongly affects the combustion efficiency and the development of the distribution of the air, fuel and products. Computational investigation of SI engines [1] has shown that higher efficiencies can be achieved if the ignition location approaches the cylinder centre when the rotational speed is over 100 rad/s. The power output and the efficiency have each been increased by 10% and 2% respectively when the spark plug is centrally located. At very low rotational speeds, the situation will be reversed. However, the results are based on computational studies only. Experimental investigation into these effects is therefore valuable.

Laboratory study often applies an impinging configuration to simulate the interaction between the flame and piston in the combustion chamber, aiming to understand the effect of the ignition location on the ignition process. McDaid and Zhang [2] demonstrated that the total ignition duration is greatly influenced by ignition location variation. Bray and Zhang [3] reported that different flame modes can be established by changing the ignition location only. In this paper, the ignition location is shown to be an important element directly affecting soot formation. Soot is a typical carbonaceous PM emission and a major hazardous air pollutant leading to considerable health detriment. For IC engines, although the quantity of soot is much less in SI engines than in diesel compression-ignition engines, the soot emission should not be overlooked. The ignition location should be carefully determined to minimise the negative impact of soot formation on engine service time and combustion efficiency. Flame temperature is another important parameter in understanding the characteristics of combustion. A modified two colour method on glowing thin silicon carbide (SiC) fibres in the flow field is used to evaluate the flame temperature in this paper.

The combustion process characteristics can be revealed via flame radical emission. Typical hydrocarbon flame emission species are distributed in the ultraviolet (UV), visible and infrared spectra [4]. In the visible spectrum, the grey-body radiation of incandescent soot leads to the flame emission of a perceptible orange

Correspondence to: yz100@sheffield.ac.uk

colour. The chemiluminescence-induced blue flame mainly consists of excited molecular radicals CH^* (430 nm) and C_2^* (Swan system, dominant emissive band head at 473.71 nm and 516.52 nm). The OH^* has the strongest band with the primary peak at 309 nm. The flame emission bands in infrared spectrum have two major peak which were subject to CO_2 and H_2O. The continuum radiation from the heated soot particles has a peak emission in the mid-infrared region. The combination of laser-based optical instruments and high-speed imaging is the most common technique to track flame radical species. However, this method is intrinsically complicated and expensive, and may require a significant redesign of the combustion chamber. Therefore a novel flame diagnostic technique, without these limitations, is introduced in this paper. This method develops from the correlation between the flame emission species and the corresponding colour distribution range in hue value established by Huang and Zhang [5]. The orange sooty flame and blue flame can be extracted separately from specific hue ranges. Wang et al. [6] reported that a high-speed camera (Photron SA4) captured a region that emitting infrared in between the blue flame and the visible sooty flame during the fuel-rich hydrocarbon ignition process. Its hue colour distribution does not overlap with the visible orange and blue flame ranges. However, infrared emission was not detected in the fuel-lean stable flame. The result demonstrated that the detected infrared emission corresponded to the soot formation and supposed to be the intermediate of the soot formation. They also found that the flame emission in blue and green channels (in the RGB model space) correlated well with the CH^* and C_2^* chemiluminescence intensities respectively. Thus the intensity ratio of the blue/green can be used to reflect the fuel and air mixing level in blue flame regions. With the help of this method, the time-dependent spatial evolutions of multiple flame emissions, which include the two chemiluminescence radicals of CH^* and C_2^*, soot and the intermediate of the soot formation that emitting in infrared, are simultaneously tracked and quantitatively analysed at variable ignition locations by using the single high-speed colour camera. Monitoring the evolution of flame light emission and temperature in combustion devices can be achieved in future by applying a borescope.

2 Experimental Procedure

2.1 Experimental setup

The schematic of the experimental setup is shown in Fig. 1. Methane and air were premixed in a mixing cylinder and then injected through a nozzle with 8.0 mm inner diameter. The gas flow rates were controlled by rotameters. Test conditions are shown in Table 1. Methane flow rate remained at 5 l/min in all cases. Air flow rate varied from 4 l/min to 12 l/min, referred as ‘Air 4’, ‘Air 8’, ‘Air 10’ and ‘Air 12’ for simplicity. The flame was ignited by a Kawasaki ignition-coil (TEC-KP02) with an output voltage of 30 kV. The spark was generated by a pair of steel electrodes with a 10 mm gap. A heavily oxidised stainless steel plate with 0.3 m diameter and 10 mm thickness was positioned at 100 mm from the nozzle exit. The ignition processes were captured by a high-speed camera (Photron FASTCAM SA4) with a full frame resolution of 1024 by 1024 pixels, 125 frame rate and 1/125s shutter speed positioned at an inclined angle to the plate. Thin filaments of SiC) were applied to measure the flame temperature. Three SiC fibres L1, L2, L3 were tightened on a frame with the distances of 20, 35 and 50 mm from the nozzle exit respectively. Another three fibres L4, L5 and L6 were suspended tautly onto the plate with a 2 mm gap, with intervals of 50 mm between fibres. The hot gas temperature can be measured according to the emission of the fibres in captured images. Since the glowing fibre was much brighter than the flame, it was impossible to image the fibre and flame simultaneously without image saturation. To overcome this issue, a Pentax stereo adapter was applied to the front of the lens to simultaneously generate two parallel images with a slight displacement. A 10-stop neutral density (ND) filter was applied to the left view which reduced the amount of light and prevented over-exposure. The right view directly captured the flame images without any filter. A pair of example images is

shown in Fig. 2 (b). With the aid of the adapter, the flame light emission and the flame temperature measurement can both be recorded simultaneously.

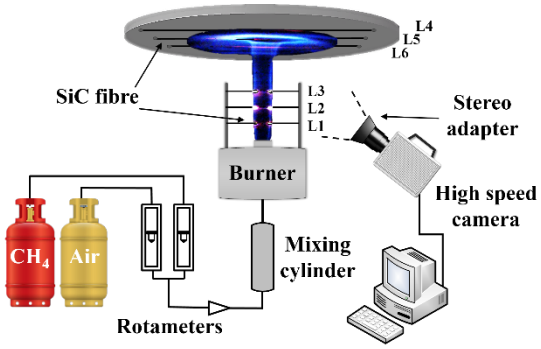

Figure 1. Experimental setup

Table 1: Test conditions

Gas type	Volume flow rate (l/min)	Velocity (m/s)	Re No.	Φ
CH_4	5	1.66	778	-
Air	4	1.37	695	2.5
Air	8	2.65	1343	1.25
Air	10	3.32	1683	1
Air	12	3.98	2018	0.83

2.2 Flame temperature measurement

Optical measurements are desirable for flame temperature monitoring because of non-intrusive, fast response, and potentially at a relatively low-cost; a modified two-colour method is thus applied to this investigation. Prior to flame temperature measurement, the two-colour has been calibrated with a standard temperature source (blackbody cavity) ranging from 973K to 1773K; the system is validated via measuring the temperature of this standard source. As shown in Fig. 3, the maximum RMS error of 5% occurred at 973K, with the average error of measured temperature at 2%. A thin SiC fibre will glow brightly in the reaction zone and will emit radiation at nearly constant emissivity, which is a requirement for two colour temperature measurement. Since fibre temperature is proportional to flame temperature, it is reasonable to determine flame temperature variation by tracking the fibre temperature. The flow disturbance caused by the fibre is negligible due to its small diameter of 15 μm.

2.3 Selective digital image enhancement technique

Our previous work reported that a high-speed camera (Photron SA4) was sensitive in the infrared region [6]. The captured infrared emission is related to the soot formation, which is supposed to be the intermediate of the soot formation process. It is well known that the CH^* and C_2^* signals along with infrared emission are weak at high shutter speeds. Selective digital image enhancement method can differentiate between the chemiluminescence-induced blue flame colorations, a band of infrared emission, and visible orange soot emission independently because they have specific hue value ranges, which are 180°~252°, 252°~330° and 10°~70° respectively. Fig. 2 (b) (right) and (f) show a comparison between the original and the enhanced flame images which demonstrate that the selective imaging enhancement is essential in revealing the combustion process in detail. Here, both the blue flame and infrared emission are enhanced 10 times, which is chosen arbitrarily to achieve the best visualisation.

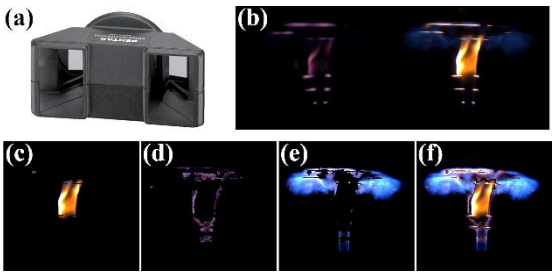

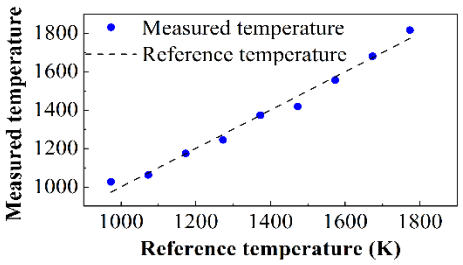

Figure 2. (a) Stereo adaptor; (b) stereo images pair, left side with ND filter; (c) visible soot emission; (d) infrared emission and (e) blue flame enhanced 10 times; (f) image after selective image enhancement.

Figure 3. Comparison between the measured and the reference temperature of blackbody calibration.

3 Results and Discussion

Under each test condition, the flame is initiated at three locations: 10 mm above the nozzle, halfway between the nozzle and plate, and the centre of the plate, named 'Nozzle', 'Middle', and 'Plate' respectively. Fig. 4 shows the image sequences of 'Air 4' cases from the flames being ignited until reaching a relative stable state. The flame characteristics are similar in the final steady state even given different ignition locations, but discrepancies are found in flame structure and colour distribution during the propagation stage. The common trend in all cases shows that the combustion process starts developing with a blue flame, followed by the infrared emission. Afterwards the sooty flame forms in orange colour. The infrared emission is found in between the blue flame and the visible sooty flame. At the early stage of ignition, the flame rapidly forms a high-temperature blue flame region. The hot gas of combustion matter obstructs the access of the air to the encircled fuel pocket. The pyrolysis of plenty of unreacted methane in the fuel pocket forms the carbon soot in the flame centre zone. The soot emits blackbody radiation in the visible spectrum and glows in orange. The intermediate of the soot formation emits in the infrared spectrum, shown as violet tints. It is noted that the soot also emits in infrared but is shadowed by the stronger visible photon emissions. Wall quenching is observed at the impinging stage due to the cool plate effect reflected by the disappearance of a large amount of CH^* and C_2^* emission. As the fuel flows continuing, the flame re-forms gradually near the plate region. Finally, the flame becomes stable with the orange soot near the plate centre, surrounded by a thin-film blue flame along the plate. The duration of ignition for 'Nozzle', 'Middle' and 'Plate' cases are 376ms, 352ms and 328ms with a maximum deviation of 8ms respectively.

Through tracking the light emission of the SiC fibres it is found that the centre of fibres L1, L2, L3 and L5 show weak visible emission because of the presence of fuel pockets. As shown in Fig. 5, each point is the average value of the temperature along a selected the length of fibre L6 during the wall quenching process. It is observed that the temperature is higher in the case of 'Nozzle' with a peak temperature 1435K at 96ms after the ignition; the cases of the 'Middle' and the 'Plate' show the maximum temperature which are 1421 K and 1415K respectively. Each case experiences a temperature drop due to the wall quenching; the most notable one is 129K found in the 'Plate' case due to the higher flame propagation velocity induced stronger convection, and the drops of 101K and 102K in 8ms in the 'Nozzle' case and the 'Middle' case respectively.

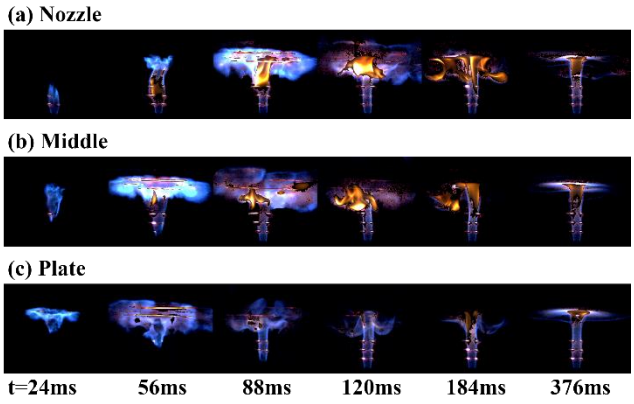

Figure 4. Image sequences of the 'Air 4' ignition process initiated at (a) the 'Nozzle', (b) the 'Middle' and (c) the 'Plate'.

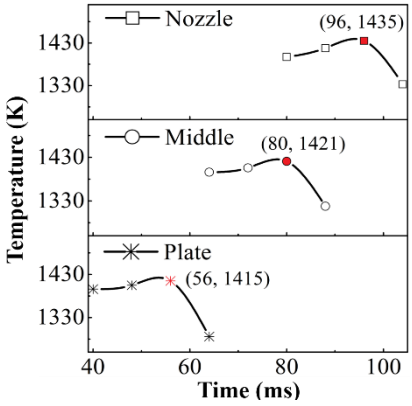

Figure 5. Fibre L6 temperature evolution of 'Air 4' in wall quenching process.

Fig. 6 (a) and (b) show the time-dependent number of pixels of the visible sooty flame and the intermediate of soot formation that emitting infrared in the 'Air 4' case. The number of pixels reflects the area occupied by the different colour regions. It is found that the quantity of soot formation rapidly increases after the wall quenching occurs. In the quenching process, the chemical reaction suddenly suspends near the plate leading to the pyrolysis of a large amount of unburnt fuel initially accumulated in the region. It can be observed that the more soot forms in the 'Nozzle' case, while the intermediate of the soot formation largely forms in the 'Middle' case, as shown in Fig. 6 (a) and (b). This may because that the 'Nozzle' ignition supplies a sufficient time for the transformation from the intermediate to the soot. In the 'Plate' case, the flame upward propagation is blocked; the effect of flame impingement is hence minimised. Therefore the quantity of soot formation and its intermediate are reduced significantly.

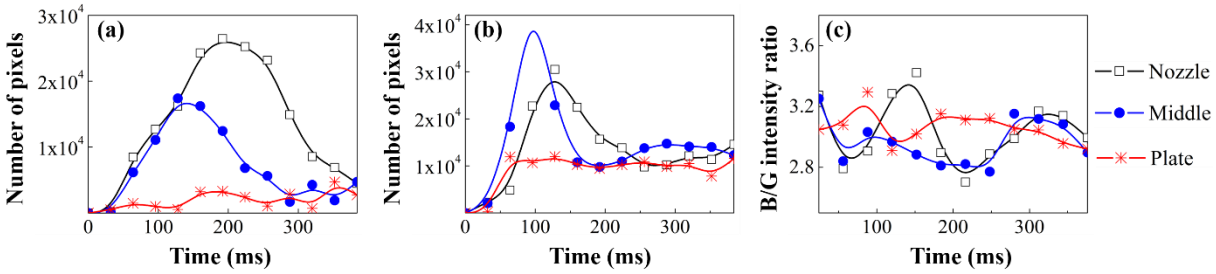

Figure 6. Time-dependent number of pixels of (a) soot-induced orange flame and (b) infrared-emission; (c) blue/green pixel intensity ratios of the chemiluminescence-induced blue flame of the 'Air 4' cases.

The time-dependent blue/green intensity ratio of the blue flame region is shown in Fig. 6 (c). Research [6] reported that the CH^* and C_2^* correlated well with the Blue and Green intensity in RGB colour model. Since CH^*/C_2^* is a function of the equivalence ratio, the intensity ratio of B/G can reflect the fuel and air mixing condition. Only the flame with a large area of the blue flame region is analysed for accuracy, which is from 24ms to 376ms. The 'Nozzle' and 'Middle' curves decline at the beginning of ignition since the flame front approaches the fuel-rich plate centre. The plate centre is the stagnation point at zero velocity, accumulating a large amount of unburnt fuel. These curves increase afterward as the flame propagates along the plate and then drop again at 152ms and 88ms due to the wall quenching. Finally, B/G ratios increase as the flame stabilise near the plate. The relative tolerances of repeated experiments are found to be less than 5%, based on the quantification of soot formation and the B/G ratio determination, which indicates good repeatability.

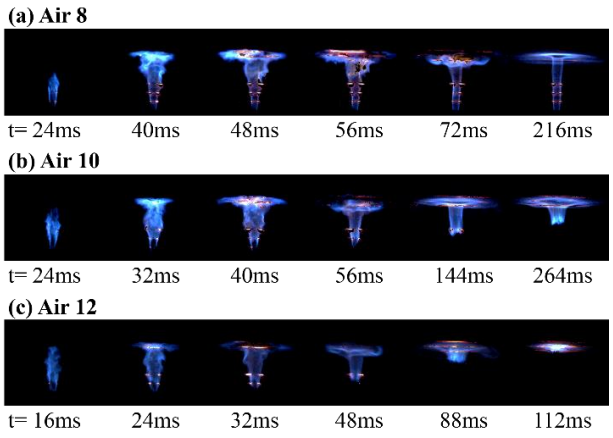

Figure 7. Image sequences of ignition processes of (a) the 'Air 8', (b) the 'Air 10' and (c) the 'Air 12' cases. The flames are initiated at the nozzle exit.

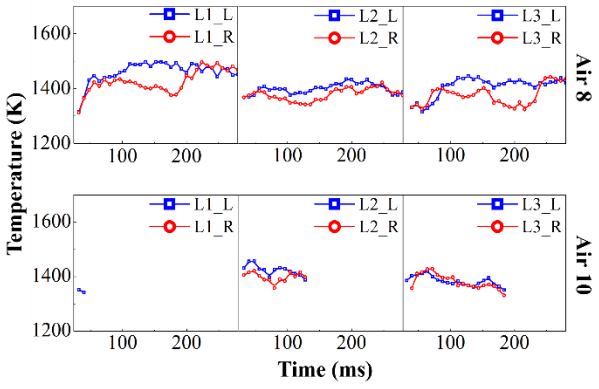

Figure 8. Time-dependent temperature variation of fibre L1, L2 and L3 initiated at nozzle in 'Air 8' and 'Air 10' cases. [L: left; R: right side of the flame]

Fig. 7 shows the image sequences of 'Air 8', 'Air 10' and 'Air 12' cases. The flames are initiated at the nozzle exit. The time-dependent temperature measurements of L1, L2 and L3 are shown in Fig. 8. With the increase of air concentration, the quantity of soot is reduced. In the 'Air 8' case, the flame right side propagation is faster than the left because of the randomness which leads to a lower flame temperature on the right side due to the faster propagation induced higher convection, as shown in Fig. 8. The temperatures of L1, L2 and L3 simultaneously drop at 56ms after ignition due to wall quenching. The flame turns to completely blue when reaching steady state with a hollow core. Detached flame is observed in the 'Air 10' case. The bottom boundary of the flame gradually leaves away from the fibres with a continuous temperature drop. As the air flow rate increases to 12 l/min, disc flame is formed which attaches to the plate. The flame temperature near the fibre L6 is approximately 1324K, 1342K and 1327K at steady state of these three cases, which indicates that the flame temperature increases when the equivalence ratio approaches unity.

4 Conclusions

The effects of ignition location on flame propagation properties and soot formation of an impinging flame have been carried out via tracking multiple light emission species and temperature by a single high speed camera. The flame temperature is evaluated using a modified two-colour method to measure the glowing thin SiC fibres positioned in the flow field. The time-dependent spatial evolutions of chemiluminescence radicals CH^* and C_2^*, soot and the intermediate of the soot formation that emitting infrared are investigated via image processing techniques. It is found that the evolution of temperature, soot formation, and chemical species are quite sensitive to ignition locations. More soot forms in the 'Nozzle' case, while the more intermediate of the soot formation forms in the 'Middle' case. The soot formation reduces greatly in the 'Plate' case. Wall quenching is observed in all cases at the impinging stage due to the cool plate effect. In the wall quenching process, the chemical reaction suddenly suspends near the plate leading to the pyrolysis of plenty of unburnt fuel initially accumulated in the region. There is more quenching-induced temperature drop in the 'Plate' case because of the strong convection resulting from higher flame propagation velocity. Detached flame and disc flame are observed when increasing the air concentration. The results show that the flame temperature increases when the equivalence ratio approaches unity.

References

[1] Medina A, Curto P, Hernández A, Guzmán L, Angulo F, Sen A. (2013). Quasi-dimensional simulation of spark ignition engines: from thermodynamic optimization to cyclic variability. Springer Science & Business Media (ISBN 978-1-4471-5288-0).

[2] McDaid C, Zhou J, Zhang Y. (2013). Experimental observations of complex flame propagations initiated at different locations of an impingement configuration. Fuel. 103: 783.

[3] Zhang Y, Bray KNC. (1999). Characterization of impinging jet flames. Combust. Flame. 116: 671.

[4] Gaydon AG. (1974). The spectroscopy of flames. Chapman and Hall (ISBN 978-94-009-5722-0).

[5] Huang HW, Zhang Y. (2011). Digital colour image processing based measurement of premixed CH_4+air and C_2H_2+air flame chemiluminescence. Fuel. 90: 48.

[6] Wang Y, Zheng L, Woolley R, Zhang Y. (2016). Investigation of ignition process from visible to infrared by a highspeed colour camera. Fuel. 185: 500.